

Two-proton radioactivity studies with ^{45}Fe and ^{48}Ni

C. Dossat,¹ A. Bey,¹ B. Blank,¹ G. Canchel,¹ A. Fleury,¹ J. Giovinazzo,¹ I. Matea,¹ F. de Oliveira Santos,² G. Georgiev,² S. Grévy,² I. Stefan,² J. C. Thomas,^{2,3} N. Adimi,⁴ C. Borcea,⁵ D. Cortina Gil,⁶ M. Caamano,⁶ M. Stanoiu,⁷ F. Aksouh,³ B. A. Brown,⁸ and L. V. Grigorenko⁹

¹*CENBG, Le Haut Vigneau, B.P.120, F-33175 Gradignan Cedex, France*

²*Grand Accélérateur National d'Ions Lourds, B.P.5027, F-14076 Caen Cedex, France*

³*Instituut voor Kern- en Stralingsfysica, Celetijnenlaan 200D, B-3001 Leuven, Belgium*

⁴*Faculté de Physique, USTHB, B.P.32, El Alia, 16111 Bab Ezzouar, Alger, Algeria*

⁵*Institute of Atomic Physics, P.O. Box MG6, Bucharest-Margurele, Romania*

⁶*Departamento de Física de Partículas, Universidad de Santiago de Compostela, E-15782 Santiago de Compostela, Spain*

⁷*Institut de Physique Nucléaire d'Orsay, 15 rue Georges Clémenceau, F-91406 Orsay Cedex, France*

⁸*Department of Physics and Astronomy and National Superconducting Cyclotron Laboratory, Michigan State University, East Lansing, Michigan 48824-1321, USA*

⁹*Flerov Laboratory of Nuclear Reactions, JINR, RU-141980 Dubna, Russia*

(Received 18 July 2005; published 22 November 2005)

In an experiment at the SISSI/LISE3 facility of GANIL, we have studied the decay of the two proton-rich nuclei ^{45}Fe and ^{48}Ni . We identified 30 implantations of ^{45}Fe and observed for the second time four implantation events of ^{48}Ni . In 17 cases, ^{45}Fe decays by two-proton emission with a decay energy of 1.154(16) MeV and a half-life of $T_{1/2} = 1.6_{-0.3}^{+0.5}$ ms. The observation of ^{48}Ni and of its decay allows us to deduce a half-life of $T_{1/2} = 2.1_{-0.7}^{+2.1}$ ms. One out of four decay events is completely compatible with two-proton radioactivity and may therefore indicate that ^{48}Ni has a two-proton radioactivity branch. We discuss all information now available on two-proton radioactivity for ^{45}Fe and ^{48}Ni and compare it to theoretical models.

DOI: [10.1103/PhysRevC.72.054315](https://doi.org/10.1103/PhysRevC.72.054315)

PACS number(s): 23.50.+z, 23.90.+w, 21.10.-k, 27.40.+z

I. INTRODUCTION

Nuclei are formed as an ensemble of protons and neutrons. They are stable against any radioactive decay only if a subtle equilibrium between the number of protons and neutrons is respected. When this condition is violated in a nucleus, it becomes radioactive. For small deviations from equilibrium, the nuclei decay by β decay. The limits of stability, the drip lines, are reached when the nuclear forces can no longer bind an ensemble of nucleons because of a too large neutron or proton excess. Nuclei beyond the proton drip line may decay from their ground states by emission of one proton for odd- Z nuclei or of two protons for even- Z nuclei. These types of radioactivity were predicted more than 40 years ago by Goldanskii [1].

One-proton radioactivity was observed for the first time in 1981 by Hofmann *et al.* [2] and Klepper *et al.* [3]. Today, almost 30 cases of one-proton radioactivity for odd- Z nuclei [4] have been identified and studied, allowing one, e.g., to determine the sequence of single particle levels and their energy beyond the proton drip line, and to investigate the tunneling process through the combined Coulomb and centrifugal barriers.

For many years, experimental studies tried to provide evidence for two-proton radioactivity, but it was only observed in the last three years in the decays of ^{45}Fe [5,6] and ^{54}Zn [7]. In this paper, we report on new results on the decay by two-proton radioactivity of ^{45}Fe , on the second observation of ^{48}Ni and, for the first time, on its decay.

II. EXPERIMENTAL TECHNIQUE

In an experiment performed in May 2004 at the SISSI-LISE3 facility of GANIL, ^{45}Fe , ^{48}Ni and about 20 less exotic proton-rich nuclei were produced by fragmentation reactions of a primary $^{58}\text{Ni}^{26+}$ beam at 74.5 MeV/nucleon. The beam, with an average intensity of 4 μA , impinged on a ^{nat}Ni target of thickness 250 mg/cm² installed in the SISSI device. The fragments were selected by the ALPHA-LISE3 separator which included a 50 μm thick beryllium degrader in the intermediate focal plane of LISE [8]. Two microchannel plate (MCP) detectors at the first LISE focal plane and a detection setup consisting of four silicon detectors installed at the end of the LISE3 beam line allowed us to identify the fragments on an event-by-event basis and to study their decay properties.

The first two silicon detectors of the telescope (300 μm) served to measure the energy loss (ΔE) of the fragments and their time-of-flight (TOF) with respect to the two MCP detectors and to the radiofrequency (RF) of the cyclotrons. The second of these detectors served also to detect β particles from the radioactive decays of the fragments stopped in the adjacent double-sided silicon-strip detector (DSSSD). The DSSSD was a 500 μm thick silicon detector with 16 x-strips on one side and 16 y-strips on the other side with a pitch of 3 mm. This detector was used to measure the residual energy of the fragments and their decay properties. Finally, the fourth element was a 5 mm thick lithium-drifted silicon detector which served to detect β particles from radioactive decays in the DSSSD. This silicon telescope allowed us to

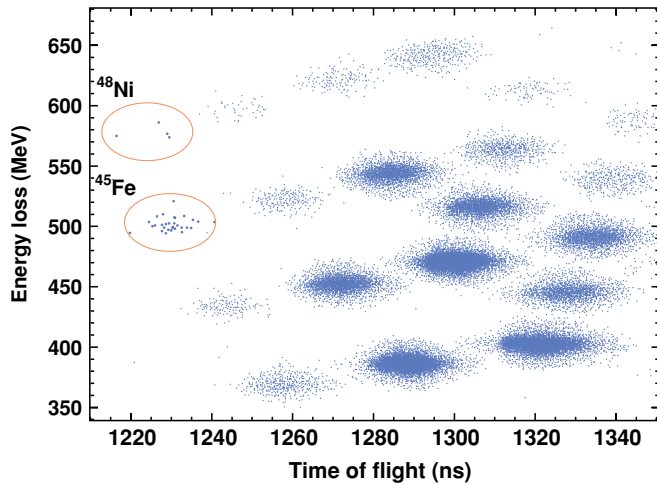


FIG. 1. (Color online) Two-dimensional identification plot for the present experiment. The implantation events are plotted as a function of their time-of-flight between the target and the first silicon detector and their energy loss in the first silicon detector. 30 ^{45}Fe and four ^{48}Ni events are unambiguously identified.

measure eight different fragment identification parameters (two ΔE signals, two residual energies from the DSSSD, and four TOF signals) which were used to unambiguously identify the different fragments and reject almost any background event (see Fig. 1). All silicon detectors were equipped with two parallel electronic chains with different gains, one for heavy-fragment identification and the other for decay spectroscopy. Triggers were generated from the first silicon detector for implantation events, from the DSSSD for charged-particle emission and from the two detectors adjacent to the DSSSD for β particles. All triggers could independently trigger the data acquisition.

The experimental data were stored on tape on an event-by-event basis. To minimize the data acquisition dead time, we used two independent CAMAC/VXI branches. The trigger to start the event treatment switched from one system to the other after each event. Both branches were read out via one VME branch. In order to avoid double triggering which sometimes occurs especially when working with leading-edge discriminators (which was the case for the DSSSD channels), we increased the trigger signal width to 20 μs . This data acquisition system allowed us to treat two subsequent events as long as they are more than 20 μs apart. The event treatment lasted about 300 μs for each of the two branches, which means that we lost one event in the case where three events arrived within 300 μs . However, these events still incremented a scaler which was read out event-by-event. Therefore, only events which followed a preceding event within less than 20 μs got completely lost.

III. EXPERIMENTAL RESULTS

A. Fragment identification

Figure 1 shows the fragment identification matrix for the present experiment. The identification procedure of the

different fragments implanted in the DSSSD can be separated in two parts [9]. First, for isotopes with a high production rate, we have determined central values and widths for the distribution of each fragment on each of the eight identification parameters. For the very exotic nuclei, we determined the position of their central values and their widths with an extrapolation for each identification parameter by using a polynomial in Z and T_Z with a maximum degree of two. Then for each event, we determined a hyper-radius R by comparing the experimental parameters P_i^{exp} with the calculated ones $P_i^{\text{cal}}(A, Z)$ normalized by the width of each parameter distribution for each isotope ${}^A Z$ considered (in total 84 ranging from $Z = 20$ to 31 and $T_Z = -1.5$ to -4.5).

The hyper-radius R was calculated for each event with respect to each isotope ${}^A Z$ by the following equation:

$$R^2(A, Z) = \sum_i \frac{(P_i^{\text{exp}} - P_i^{\text{cal}}(A, Z))^2}{\sigma_i^2(A, Z)}, \quad (1)$$

where A and Z are the mass and charge number of a given isotope, σ_i is the width of the distribution of parameter i . It was found that, without introducing a significant error, the width for each parameter could be assumed to be the same for all isotopes: $\sigma_i(A, Z) = \sigma_i$.

Implantation events were accepted, if their associated hyper-radius R for the whole parameter space was smaller than a fixed hyper-radius R_{max} . The value of R_{max} was chosen to minimize the number of isotopes rejected, but also to minimize the number of multiple and “wrong” identifications, i.e., “identifications” of nuclei which are known to be particle unstable. In the present analysis, all eight parameters of an event had to lie on average within three standard deviations of the predefined values. This identification method allowed us to attribute 30 implantation events to ^{45}Fe and four to ^{48}Ni .

B. The decay of ^{45}Fe

Figure 2 shows the decay energy spectrum measured for the first decay event in the same x - y pixel after a ^{45}Fe implantation. For 30 implantations, we observed 17 decay events with a decay energy of 1.154(16) MeV. We start with the assumption that this peak is due to two-proton radioactivity of ^{45}Fe . In the

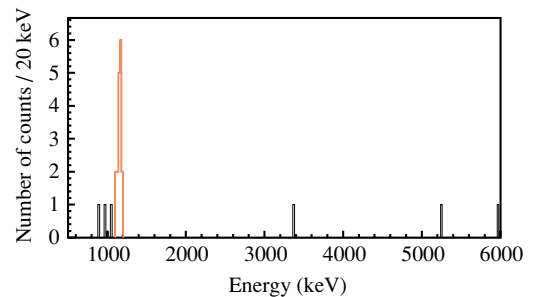


FIG. 2. (Color online) Decay energy spectrum for the first decay event in the same pixel after an implantation of ^{45}Fe . A decay energy of 1.154(16) MeV is determined from the seventeen events in the peak. Events with an energy release above 6 MeV are cut in the figure.

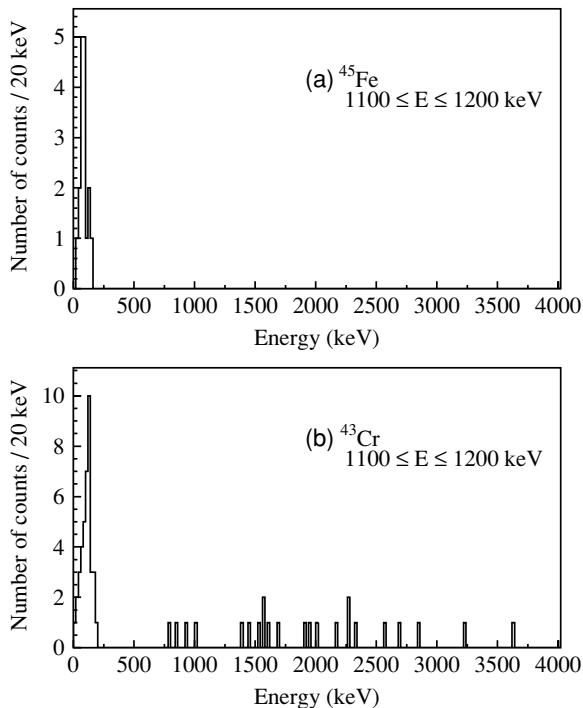


FIG. 3. (a) Energy spectrum from the last silicon detector obtained in coincidence with events in the peak at 1.154 MeV (see Fig. 2) from the decay of ^{45}Fe . No β signal beyond the detector noise is observed. For this plot, we excluded the event discussed in detail in the text. (b) Same spectrum in coincidence with a signal between 1.1 and 1.2 MeV for ^{43}Cr . Similar spectra were obtained also with the detector in front of the DSSSD.

following, we will accumulate experimental evidence for this assumption.

First of all, none of these 17 events has a coincident β signal in the adjacent detectors [Fig. 3(a)], whereas the β -particle signals can be observed for neighboring nuclei (e.g., ^{43}Cr) which disintegrate by β decay [Fig. 3(b)]. The detection efficiency for β particles in the two detectors adjacent to the DSSSD was determined via β particles from the decay of known β -delayed proton emitters like ^{52}Ni . We obtained values of 40(5)% for the Si(Li) detector and of 20(10)% for the detector in front of the DSSSD. With these values, we determine a probability to miss all β particles, if the 1.154 MeV peak were of a β -delayed origin, of less than 4×10^{-5} (one-sigma limit). In addition, as in our previous experiment [5], the full width at half-maximum of the 1.154 MeV peak is much narrower [46(17) keV] as, e.g., the β -delayed proton peak at 1.75 MeV of ^{40}Ti [76(3) keV], which indicates that no β pile-up contributes to the width of the 1.154 MeV peak.

Another piece of evidence comes from the fact that the second decay after ^{45}Fe implantation is compatible with the decay of ^{43}Cr , the $2p$ daughter of ^{45}Fe . We determine a half-life of 18_{-4}^{+6} ms for the second decay which has to be compared to the value measured from decay events after ^{43}Cr implantation of 20.8(3) ms [9,10]. In addition, ^{43}Cr decays mainly by β -delayed protons with charged-particle energies in the range

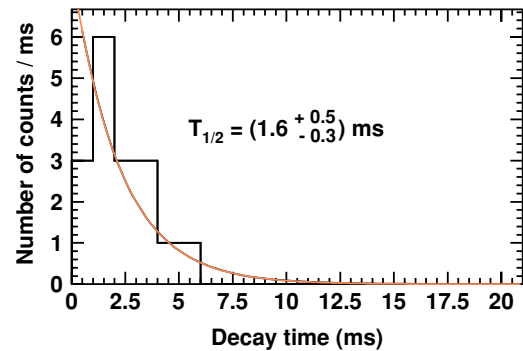


FIG. 4. (Color online) Decay time spectrum for the first decay event after ^{45}Fe implantation with a decay energy in the 1.154 MeV peak. A maximum likelihood fit yields a half-life of $1.6_{-0.3}^{+0.5}$ ms.

of 2–5 MeV. This is exactly what is observed for the second decay after ^{45}Fe implantation.

The accumulated experimental evidence can consistently be explained only by an important $2p$ branch in the decay of ^{45}Fe . All other possible decay modes like β -delayed decays, direct one-proton emission or α decay can be excluded with a rather high probability. For example, the Coulomb barrier penetration half-life for α decay with a decay energy of 1.154 MeV is about 140 s. Similarly, a one-proton emission with this decay energy has a barrier penetration half-life of 10^{-17} s. Therefore, both processes can safely be excluded.

Figure 4 shows the decay-time spectrum for the first decay event after ^{45}Fe implantation, where we requested the energy signal to be in the peak at 1.154 MeV. The half-life fit yields a value of $1.6_{-0.3}^{+0.5}$ ms. A fit of all first decay events gives a value of $1.4_{-0.2}^{+0.3}$ ms. As the half-life value from this experiment, we will keep the value we obtained from the spectrum conditioned by the 1.154 MeV peak. This value is somewhat lower than previously published values, but still in the acceptable range (see below).

We excluded one first decay event after ^{45}Fe implantation from the analysis described so far. This event has a decay energy of 1.15 MeV and lies therefore nicely in the $2p$ peak. However, the decay takes place 46 ms after the implantation. If we assume a half-life of the order of 2–4 ms [5,6], we find a probability of 10^{-6} – 10^{-3} for such a decay to take place after 40 ms. In addition, the second decay for this implantations event happens after about 575 ms. There is again a rather low probability (6×10^{-8}) for such an event after 500 ms to be due to a decay of ^{43}Cr which has a half-life of 20.8(3) ms [9,10]. Finally, the energy signal in the adjacent β detector for the first decay event is 950 keV and therefore in a region where the signals for real β events start [see Fig. 3(b)].

From an inspection of the scaler contents, we are sure that we did not miss events between the implantation of this ^{45}Fe and its subsequent decays, except if the first decay took place less than 20 μs after the implantation event, which is rather unlikely for a half-life in the few ms range, or after any following event. We cannot exclude this second possibility, as there were 15 events registered between the implantation of this ^{45}Fe nucleus and the observation of the first decay in the same pixel. One of these events, which occur in other

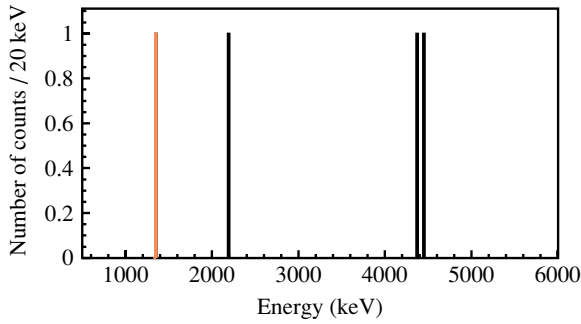


FIG. 5. (Color online) Decay energy spectrum for the first decay event after a ^{48}Ni implantation. The count at 1.35(2) MeV may be of two-proton origin.

pixels, may have blocked the data acquisition and the scalers in order to miss the first decay event. Therefore, as the observed parameters, i.e., the decay time, the daughter decay time, and the β energy, make it rather unlikely that this first observed decay event is really the first decay event which took place, we excluded it from any further analysis. The decay energy, which is compatible with the $2p$ peak of ^{45}Fe , could also be attributed to the decay of ^{43}Cr , which has an important part of its decay strength in this energy region [9,10]. Finally, another possible cause could be that the implantation event was wrongly attributed to ^{45}Fe , which could be due to a heavy ion which is not completely stripped. However, as such a heavy ion has most likely to keep the same charge state after the target and the degrader, we believe that this probability is low (much less than 1%).

Our final results for the decay of ^{45}Fe are a $2p$ decay energy of 1.154(16) MeV, a half-life of $1.6_{-0.3}^{+0.5}$ ms, and a $2p$ branching ratio of 0.57(10).

C. The decay of ^{48}Ni

For ^{48}Ni , four implantation events have been identified. They are correlated with subsequent decay events. Figure 5 shows the decay energies of the first decay events in the same pixels. It can be excluded that the counts above 2 MeV are of two-proton radioactivity origin. They would lead to a barrier penetration half-life that is far too short, when compared with the measured half-life (see below). However, the event at 1.35(2) MeV lies in the region where two-proton radioactivity of ^{48}Ni would be expected (see below). In addition, this event has no coincident β particle. The decay happens after 1.66 ms. It is followed by a charged-particle emission with an energy release of 4.748(20) MeV after 1.03 ms. This delay may be compared to the half-life of the $2p$ daughter nucleus of ^{48}Ni , ^{46}Fe , which has a half-life of 10.3(15) ms [9,10]. The β -delayed one-proton and two-proton emitters ^{47}Fe and ^{46}Mn , two other possible daughters, have half-lives of 21.6(4) ms and 34.4(7) ms [9,10], respectively.

Figure 6 shows the decay-time spectrum. From the four decay events, we determine a half-life of $2.1_{-0.7}^{+2.1}$ ms. For one implantation of ^{48}Ni , we lost two events between the implantation and the first observed decay in the same pixel. These events have been registered by the scalers, but not by

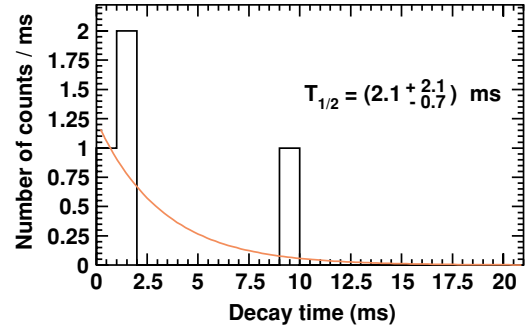


FIG. 6. (Color online) Decay time spectrum for ^{48}Ni . The spectrum shows the time for the first decay event after the implantation of an identified ^{48}Ni nucleus. A half-life of $T_{1/2} = 2.1_{-0.7}^{+2.1}$ ms is determined.

the data acquisition. It might therefore be that the half-life of ^{48}Ni is even a little shorter, although it was not necessarily the decay of ^{48}Ni , which we missed, but possibly another implantation or decay event. We favor this last explanation, as the observed decay happens after only 1.1 ms. We did not determine a half-life for a possible daughter decay, as different decay branches and therefore different daughter half-lives most likely are present.

The decay data measured for ^{48}Ni may be interpreted as a branch of $25_{-19}^{+29}\%$ for $2p$ radioactivity and yield, if assumed to be $2p$ radioactivity, a partial half-life of $8.4_{-7.0}^{+12.8}$ ms. However, such possible evidence is of course far from constituting a definite observation of $2p$ radioactivity for ^{48}Ni . Rather we believe that more statistics is required to confirm or reject such an assumption. We will nonetheless compare this result with theory below, as the agreement or disagreement with a theory tested now for ^{45}Fe and ^{54}Zn may shed some light on the likelihood of a possible $2p$ origin of the event at 1.35 MeV.

IV. DISCUSSION AND COMPARISON TO THEORY

A. Theoretical models

A first comparison between predictions and experiment will consist in confronting experimental $2p$ Q values with theoretical predictions. We will use the models from Brown [11], Cole [12], and Ormand [13,14].

Brown's prediction is based on the isobaric multiplet mass equation (IMME), which allows one to determine the mass of a proton-rich nucleus from its neutron-rich mirror by either determining the coefficients of the IMME experimentally via mass measurements or by calculating the b coefficient with theoretical models. Brown used a shell-model approach which includes an isospin nonconserving Hamiltonian to determine b . Only the $1f_{7/2}$ orbital was included in the study. A "weak-coupling" scheme was used for cross-shell nuclei.

A similar approach was employed by Ormand [13,14]. However, he used a more advanced isospin nonconserving interaction and the full fp model space.

Cole [12] also used the IMME as a starting point. To determine the difference in mass between a proton-rich nucleus and its neutron-rich mirror, he employed directly the Coulomb

TABLE I. Decay energies, half-lives, branching ratios, and partial half-lives as determined in three independent experiments for the decay of ^{45}Fe . The average values represent the error weighted averages of the three experimental values. To get agreement within error bars, the errors of the half-lives have been inflated by a factor of 1.07.

	$2p$ decay energy (MeV)	Half-life (ms)	Branching ratio	Partial half-life (ms)
Giovinazzo <i>et al.</i> [5]	1.140 ± 0.040	$4.7_{-1.4}^{+3.4}$	0.55 ± 0.12	$8.5_{-3.2}^{+6.4}$
Pfützner <i>et al.</i> [6]	1.1 ± 0.1	$3.2_{-1.0}^{+2.6}$	$0.80_{-0.25}^{+0.15}$	$4.0_{-1.8}^{+3.3}$
This work	1.154 ± 0.016	$1.6_{-0.3}^{+0.5}$	0.57 ± 0.10	$2.8_{-0.7}^{+1.0}$
Average	1.151 ± 0.015	$1.75_{-0.28}^{+0.49}$	0.59 ± 0.07	$3.0_{-0.6}^{+0.9}$

energy differences between the two nuclei. For this purpose, Cole used a parametrization of the Coulomb displacement energies.

Beyond this Q value comparison, we will confront our results also with more refined models which link decay energy and decay half-life by including nuclear structure and nuclear dynamics. However, for the moment no model can consistently include both. The first model we will present contains to a large extent the nuclear structure needed to correctly treat the $2p$ emission process, however, it contains no dynamics. The second model treats the emission process dynamically, but has to use approximations in other respects (see below).

Starting from the traditional R -matrix approach for one-proton capture or emission, Brown and Barker developed an R -matrix model which can be applied for $2p$ emission [15,16]. This model includes the proton-proton interaction as an s -wave intermediate state. The nuclear structure input is the spectroscopic factor [17] $S = (\frac{A}{A-2})^\lambda G^2(pf) C(A, Z)$, where $G^2 = 5/16$, $\lambda = 6$, A is the mass of the parent nucleus, and $C(A, Z) = |\langle \Psi(A-2, Z-2) | \psi_c | \Psi(A, Z) \rangle|^2$ is the spectroscopic factor for the cluster overlap of a diproton wavefunction ψ_c in the pf shell with $L = 0$, $S = 0$, and $T = 1$ in the SU3 basis.

The spectroscopic factors were obtained with the GPFX1 interaction [18] for ^{45}Fe ($C = 0.33$) and ^{48}Ni ($C = 0.24$). For the diproton-nucleus potential, we take a Woods-Saxon form plus a uniform-sphere Coulomb potential with radius $R_C = r_C A^{1/3}$. The Woods-Saxon parameters are $R = r_0 A^{1/3}$ for the radius, a_0 for the diffuseness, and a well depth adjusted to reproduce the binding energy. The potential parameters are taken from an analysis of low-energy deuteron scattering [19]: $r_0 = 1.17$ fm, $a_0 = 0.72$ fm, $r_C = 1.30$ fm. We will use this model to compare our experimental results to theory.

The other model which allows one to perform a comparison between theory and experiment is the three-body model of Grigorenko *et al.* [20,21]. It uses the hyperspherical harmonics approach to treat the decay of a three-body system consisting of two protons and a structureless core. This model calculates first a “box” wave function for a finite domain, which is then used as a source for the wave function for the decay particles. The Pauli principle is taken into account approximately via repulsive cores for occupied orbitals. The influence of nuclear structure on the decay width of the decaying nucleus can be studied in the model phenomenologically by a variation of the effective core-proton interactions. This allows one to generate wave functions with different population of the dominating shell-model configurations (in the case of ^{45}Fe and ^{48}Ni with

different ratios of p^2 and f^2 configurations). This treatment of the structure has essentially single-particle character and may possibly miss some important many-body effects. The cases of pure p^2 and f^2 form boundaries for the possible lifetime values. Other features of the model are the dynamical treatment of the pairing interaction below the barrier which is introduced in the form of realistic proton-proton potentials and the opportunity to calculate momentum distributions for the decay products [22].

In the future, it will also be interesting to compare the experimental data to the results of the shell-model embedded in the continuum [23]. However, no theoretical results from this model for the cases discussed here are presently available.

B. Comparison between experiment and theory for ^{45}Fe

The decay of ^{45}Fe has been observed now in three different experiments. Table I gives the experimental results for the $2p$ decay energy, the half-life, the branching ratio, and the partial half-life for the $2p$ branch. The average of these results will be compared to theory. The average experimental Q value for $2p$ radioactivity of ^{45}Fe of 1.151(15) MeV may be compared to the predictions of the three models described above. Brown [11] gives a value of 1.154(94) MeV, whereas Ormand finds a Q value of 1.279(181) MeV. Both values are in nice agreement with our experimental value. Cole’s calculations result in a value of 1.218(49) MeV, which is in reasonable agreement with our experimental result.

These results show that models tailor-made for the mass region of interest nicely reproduce our experimental results. Therefore, it seems to be reasonable to assume that the same models also should have some predictive power for new $2p$ radioactivity candidates in the same region.

The R -matrix model of Brown and Barker [16] yields a half-life of 46_{-16}^{+25} ms. Ignoring the p - p resonance gives a result of 14_{-4}^{+12} μs (see Fig. 7). As in the case of ^{54}Zn [7], the experimental decay rate is faster than the theoretical value calculated by taking the p - p resonance into account. In the present case, the experimental partial half-life for $2p$ radioactivity is about a factor of 15 faster. As described in Ref. [16], a qualitative explanation might be the contribution from major shells below and above the major shell considered in the model. In Ref. [24], an enhancement factor of about two (the ratio of the ϵ factors in columns 3 and 5 of Table 3 of that paper) due to mixing with the sd and $g_{9/2}$ orbitals was calculated for the two-neutron transfer in the (p, t) reaction in the pf shell. Another explanation might also be that basically no

TABLE II. The experimental $2p$ decay energy of ^{48}Ni is compared to different model predictions which were, in part, already used for ^{45}Fe . All predictions are in agreement with the experimental value. All data are in MeV.

Experimental decay energy	Brown [11]	Cole [12]	Ormand [13]	Ormand [14]	Nazarewicz <i>et al.</i> [25]
1.35 ± 0.02	1.36 ± 0.13	1.35 ± 0.06	1.14 ± 0.21	1.29 ± 0.33	0.0–2.0

decay dynamics is included in this model. However, to refine these conclusions more theoretical and experimental work is necessary.

Figure 7 compares the experimental mean values for the partial half-life and the decay Q value to the model predictions of Grigorenko and co-workers [21,22]. The experimental value lies in between the three-body predictions for the limiting cases of pure p^2 and f^2 configurations for the internal structure of ^{45}Fe . From a standard shell model, one would expect the last two protons to be in the $f_{7/2}$ orbital. However, it is well known that a $p_{3/2}$ contribution from the next shell may have a significant influence on the barrier penetration half-life. The experimental results are consistent with p^2 configuration weights from 100% to 40% (see Fig. 6 from Ref. [22]). Therefore, we conclude that the experimental datum is in agreement with the theoretical predictions from the three-body model.

In Fig. 7, we compare our result also to the simple diproton model, which assumes that the two protons are emitted as a ^2He particle without any internal structure. This corresponds to the R -matrix approach when we neglect the p - p interaction. It is evident that this diproton model gives only an upper limit for the decay width for a given decay energy.

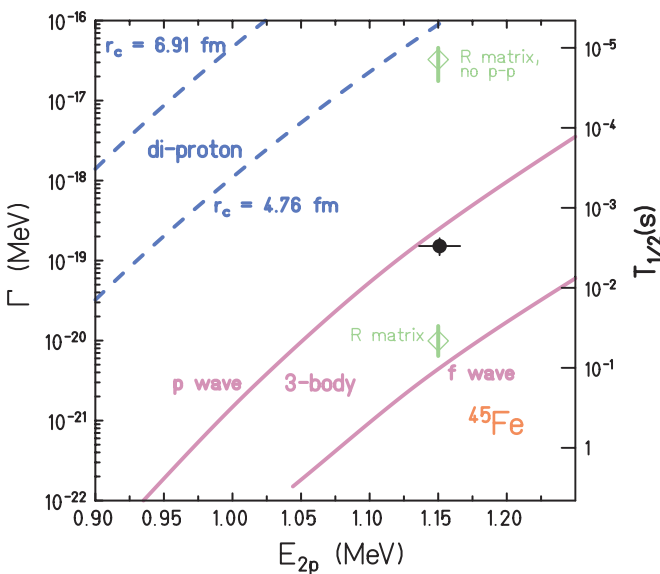


FIG. 7. (Color online) Comparison of our experimental data point for ^{45}Fe with the three-body model of Grigorenko and co-workers [21,22] for p -wave and f -wave emission and with the diproton model for two different channel radii in the R -matrix sense. In addition, we present also the results from the R -matrix approach of Brown and Barker [16] with and without the p - p resonance.

C. Comparison between experiment and theory for ^{48}Ni

Table II compares the decay energy measured for the possible $2p$ event of ^{48}Ni with theoretical predictions for this decay energy. We use the same models as for ^{45}Fe above and added a comparison to prediction from Nazarewicz and co-workers [25] who used HFB calculations with different effective interactions to predict $2p$ Q values. Depending on the interaction used values between zero, i.e., a bound ^{48}Ni , and 2.0 MeV were obtained.

The other models are in nice agreement with our experimental datum. This agreement between different model predictions and our experimental value from the possible $2p$ event may be interpreted as an additional indication that the observed event may be indeed of $2p$ origin.

The experimental half-life of $2.1_{-0.7}^{+2.1}$ ms is short compared to the β -decay half-life prediction of Ormand [13] of 9 ms. It may indicate that this theoretical β -decay half-life is only a partial half-life.

With the experimental Q value of 1.35(2) MeV, the resulting half-life in the Brown-Barker R -matrix model is 16_{-4}^{+10} ms, whereas the value is 8_{-3}^{+4} μs when the p - p resonance is ignored. As in the cases of ^{45}Fe and of ^{54}Zn [7], the experimental decay rate is faster than the theoretical value which takes into account the p - p resonance. If one accepts the assumption that the decay event observed in the present experiment is indeed a $2p$ decay of the ground state of ^{48}Ni , the experimental partial decay half-life of $8.4_{-7.0}^{+12.8}$ ms is about twice as fast as the theoretical value. However, in spite of the large uncertainties we prefer rather to state that the theoretical result does not contradict our assumption of one decay event of ^{48}Ni being of two-proton nature.

A comparison to the three-body model of Grigorenko *et al.* shows again nice agreement between our experimental point and the calculations. The experimental datum is between the two extremes of pure p -wave emission and pure f -wave emission, as it was in the case of ^{45}Fe and ^{54}Zn .

V. CONCLUSION

In this paper, we have presented new results on the decay of ^{45}Fe and first decay results for ^{48}Ni . The ^{45}Fe data show again clear evidence for two-proton radioactivity. Our present results are combined with earlier results for the decay of this nucleus to yield error weighted averages for the decay energy (1.154 ± 0.015 MeV), the half-life ($1.75_{-0.28}^{+0.49}$ ms), the branching ratio (0.59 ± 0.07), and the partial half-life for two-proton radioactivity ($3.0_{-0.6}^{+0.9}$ ms). We compared these values to model predictions and found good agreement.

The decay of ^{48}Ni was observed for the first time in the present work. We determined a half-life of $T_{1/2} = 2.1_{-0.7}^{+2.1}$ ms.

Out of the four decay events correlated to a ^{48}Ni implantation, one event is in agreement with what is expected for a $2p$ decay. This event has an energy release of 1.35(2) MeV. A comparison to $2p$ radioactivity models confirms the possibility that ^{48}Ni may decay with a small branching ratio by $2p$ radioactivity. However, better statistics is necessary to confirm or reject this hypothesis.

Future experiments will try to improve the results obtained up to now for ^{54}Zn [7] and especially for ^{48}Ni , to search for further $2p$ emitters with ^{59}Ge being a good candidate, and to study the decay process itself with an improved setup. For

this purpose, time-projection chambers are ideally suited and under construction.

ACKNOWLEDGMENTS

We would like to acknowledge the continuous effort of the whole GANIL staff and in particular of the LISE group for ensuring a smooth running of the experiment and for replacing all the broken targets. This work was supported in part by the U.S. National Science Foundation under Grant No. PHY-0244453 and by the Conseil Régional d'Aquitaine.

-
- [1] V. I. Goldanskii, Nucl. Phys. **19**, 482 (1960).
 [2] S. Hofmann *et al.*, Z. Phys. A **305**, 111 (1982).
 [3] O. Klepper *et al.*, Z. Phys. A **305**, 125 (1982).
 [4] P. J. Woods and C. N. Davids, Annu. Rev. Nucl. Part. Sci. **47**, 541 (1997).
 [5] J. Giovannozzo *et al.*, Phys. Rev. Lett. **89**, 102501 (2002).
 [6] M. Pfützner *et al.*, Eur. Phys. J. A **14**, 279 (2002).
 [7] B. Blank *et al.*, Phys. Rev. Lett. **94**, 232501 (2005).
 [8] A. C. Mueller and R. Anne, Nucl. Instrum. Methods Phys. Res. B **56**, 559 (1991).
 [9] C. Dossat, Ph.D. thesis, University Bordeaux I, unpublished (2004).
 [10] C. Dossat *et al.*, to be published.
 [11] B. A. Brown, Phys. Rev. C **43**, R1513 (1991).
 [12] B. J. Cole, Phys. Rev. C **54**, 1240 (1996).
 [13] W. E. Ormand, Phys. Rev. C **53**, 214 (1996).
 [14] W. E. Ormand, Phys. Rev. C **55**, 2407 (1997).
 [15] F. C. Barker, Phys. Rev. C **63**, 047303 (2001).
 [16] B. A. Brown and F. C. Barker, Phys. Rev. C **67**, 041304(R) (2003).
 [17] N. Anyas-Weiss *et al.*, Phys. Rep. **12**, 201 (1974).
 [18] M. Honma, T. Otsuka, B. A. Brown, and T. Mizusaki, Phys. Rev. C **69**, 034335 (2004).
 [19] W. W. Daehnick, J. D. Childs, and Z. Vrcelj, Phys. Rev. C **21**, 2253 (1980).
 [20] L. V. Grigorenko, Y. Fujiwara, M. Kohno, C. Nakamoto, and Y. Suzuki, Phys. Rev. C **64**, 054001 (2001).
 [21] L. V. Grigorenko and M. V. Zhukov, Phys. Rev. C **68**, 054005 (2003).
 [22] L. Grigorenko, I. Mukha, and M. Zhukov, Nucl. Phys. **A714**, 425 (2003).
 [23] J. Rotureau, J. Okolowicz, and M. Ploszajczak, Phys. Rev. Lett. **95**, 042503 (2005).
 [24] P. Decowski, W. Benenson, B. A. Brown, and H. Nann, Nucl. Phys. **A302**, 186 (1978).
 [25] W. Nazarewicz, J. Dobaczewski, T. R. Werner, J. A. Maruhn, P. G. Reinhard, K. Rutz, C. R. Chinn, A. S. Umar, and M. R. Strayer, Phys. Rev. C **53**, 740 (1996).